A scalable solvent-exchange strategy for the drying of colorless Japanese cedar (Cryptomeria japonica)

Yi Hien Chin, Yoshiki Horikawa, Christophe Vial, Joseph Gril, Rostand Moutou Pitti, Salah-Eddine Ouldboukhitine, Nicolas Labonne, Pascal Biwole

▶ **To cite this version:**

Yi Hien Chin, Yoshiki Horikawa, Christophe Vial, Joseph Gril, Rostand Moutou Pitti, et al.. A scalable solvent-exchange strategy for the drying of colorless Japanese cedar (Cryptomeria japonica). Drying Technology, 2025, 43 (3), pp.510-526. ⟨10.1080/07373937.2024.2434890⟩. ⟨hal-04826936⟩

HAL Id: hal-04826936

https://hal.science/hal-04826936v1

Submitted on 9 Dec 2024

HAL is a multi-disciplinary open access archive for the deposit and dissemination of scientific research documents, whether they are published or not. The documents may come from teaching and research institutions in France or abroad, or from public or private research centers.

L'archive ouverte pluridisciplinaire **HAL**, est destinée au dépôt et à la diffusion de documents scientifiques de niveau recherche, publiés ou non, émanant des établissements d'enseignement et de recherche français ou étrangers, des laboratoires publics ou privés.

Distributed under a Creative Commons CC BY-NC-ND 4.0 - Attribution - Non-commercial use - No Derivative Works - International License

Yi Hien Chin, Yoshiki Horikawa, Christophe Vial, Joseph Gril, Rostand Moutou Pitti, Salah-Eddine Ouldboukhitine, Nicolas Labonne & Pascal Biwole (06 Dec 2024): A scalable solvent-exchange strategy for the drying of colorless Japanese cedar (Cryptomeria japonica), Drying Technology, DOI: 10.1080/07373937.2024.2434890

A scalable solvent-exchange strategy for the drying of colorless Japanese cedar (*Cryptomeria japonica*)

Yi Hien Chin[a,b], Yoshiki Horikawa[c], Christophe Vial[a], Joseph Gril[a,d], Rostand Moutou Pitti[a,e], Salah-Eddine Ouldboukhitine[a], Nicolas Labonne[b], and Pascal Biwole[a,f,g]

[a]Université Clermont Auvergne, CNRS, Clermont Auvergne INP, Institut Pascal, Clermont-Ferrand, France; [b]Dagard Company, Boussac, France; [c]Institute of Agriculture, Tokyo University of Agriculture and Technology, Fuchu, Japan; [d]Université Clermont Auvergne, INRAE, PIAF, Clermont-Ferrand, France; [e]CENAREST, IRT, Libreville, Gabon; [f]Mines Paris, PSL University, Center for Processes, Renewable Energy and Energy Systems (PERSEE), Sophia Antipolis, France; [g]California State Polytechnic University, Humboldt, School of Engineering, Arcata, CA, USA

ABSTRACT

The thermal insulation properties of wood can be improved by wood modification nanotechnology, but scaling up drying techniques remains a challenge. This study aims to enhance the industrial feasibility of drying colorless (lignin-free) wood by solvent-exchange strategy. In this work, the delignification of Japanese cedar wood was applied through combined organosolv and sodium chlorite bleaching, and different drying techniques were compared to analyze their effects on porosity and dimensional stability, with water, ethanol, or acetone as solvents. The results show that the dimensional stability of colorless wood is strongly influenced by the liquid's surface tension in the porous structure. Ethanol-exchanged samples dried at 80 °C showed the best balance between drying efficiency and preservation of wood structure, reducing density to 0.16 g cm^3 and increasing specific surface area to 7.2 m^2 g^{-1}. The results describe how the drying step is optimized for the potential large-scale production of functionalized wood scaffolds or bio-based thermal insulators. The findings contribute to understanding colorless wood drying mechanisms and guide the selection of appropriate techniques for desired end-use properties, advancing wood modification nanotechnology.

GRAPHICAL ABSTRACT

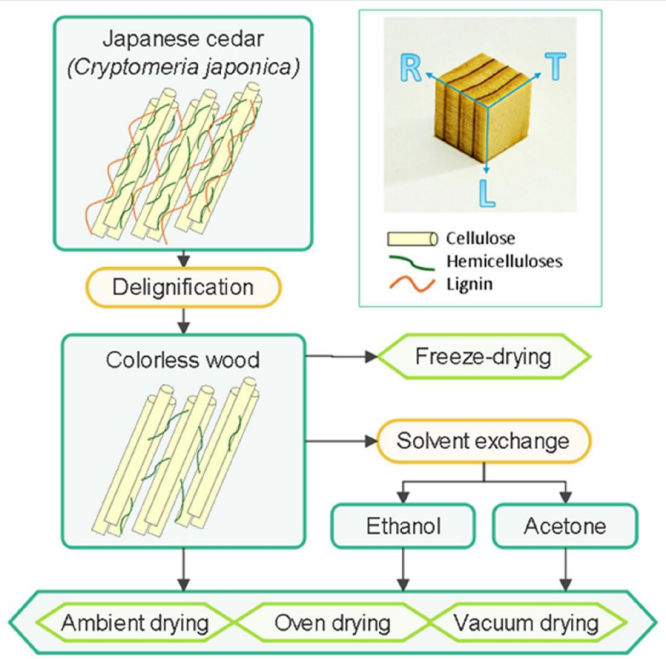

ARTICLE HISTORY
Received 8 September 2024
Revised 14 November 2024
Accepted 23 November 2024

KEYWORDS
Bio-based material; delignification; drying technologies; Japanese cedar; solvent exchange

CONTACT Yi Hien Chin yi_hien.chin@uca.fr Université Clermont Auvergne, CNRS, Clermont Auvergne INP, Institut Pascal, Clermont-Ferrand, France

Introduction

Achieving the Sustainable Development Goals requires a significant reduction in CO_2 and greenhouse gas emissions in the building industry.[1] One strategy to achieve this is to substitute nonrenewable building materials with bio-based products that have low embodied energy. Wood has always been used in construction because of its availability, ease of manipulation, structural load-bearing capacity, and ability to provide a comfortable indoor environment. For example, balsa wood, known for being the lightest wood in the world, is used as a thermal insulator with carbon storage capabilities. However, importing this wood species from distant continents contributes to higher transportation-related CO_2 emissions. Wood modification nanotechnologies inspired by the paper pulping industry aim to enhance the thermal insulating properties of local wood species. By removing non-cellulosic substances without defibrillating cellulose microfibrils, delignified wood can achieve a transverse thermal conductivity in the range of 0.028–0.051 $W\ m^{-1}\ K^{-1}$, positioning it as a potential biodegradable thermal insulator.[2–5] However, maintaining the dimension integrity of delignified wood at both the microscale and macroscale requires freeze-drying or supercritical drying, which allows preservation of the newly created microcracks and nanopores. These drying techniques are not suitable for large-scale applications due to the size limitations of the instruments required to create a differential pressure environment. Direct oven drying of water-saturated modified wood can cause excessive shrinkage and cell wall collapse due to drying stresses during water evaporation. The final porosity is highly influenced by the drying method, and freeze-dried modified wood were reported to have 13% higher porosity than oven-dried modified wood.[6] Exchanging water in modified wood with a solvent of lower surface tension reduces capillary pressure in pores, thus preventing cell wall collapse.[5,7] In particular, the additional solvent exchange step using ethanol, acetone, and pure butanol before freeze-drying can minimize the drying stress.[8] A specific surface area (SSA) of up to 41 $m^2\ g^{-1}$, indicating increased porosity compared with that of natural wood, was reported in ethanol-exchanged delignified wood dried under supercritical CO_2.[9] Solvent exchange by hexane was used in the nanocellulose production, both in gel and solid wood forms.[7,10] Ambient drying of ethanol-exchanged modified wood has also been reported to produce "white wood" or "insulwood" with improved porosity.[5,11]

Despite the numerous potential applications of delignified wood described in the literature, a thorough comparative analysis of alternative drying techniques is still lacking, leaving it unclear which scalable method is the most suitable for drying delignified wood. To date, the feasibility of scaling-up the industrial production of delignified wood has not been established, especially concerning the drying step in manufacturing. Due to the significant energy consumption of the drying process, a comprehensive understanding is needed before industrial implementation. Few scientific works have focused on the drying mechanisms of porous delignified wood and current drying technologies face limitations in industrial applications, particularly in preserving wood porosity. This study aims to explore a scalable solvent-exchange drying technique to address these challenges.

The objective of this study is to determine the optimal drying process by comparing different solvents and drying methods, aiming to enhance colorless (lignin-free) wood dimensional stability and porosity for industrial-scale applications. Organosolv pulping *via* alcoholysis treatment was reported to produce lignin-free wood after sodium chlorite bleaching.[12] This study first examines the delignification protocol by analyzing its impact on the chemical constituents and the cellulosic structure of Japanese cedar wood blocks. After non-cellulosic component extraction, the optimal conditions for the evaporation of the solvent in the solvent-exchanged lignin-free Japanese cedar wood blocks were determined. The selection of solvent exchange drying techniques for experimentation was motivated by the potential application for large-scale production and the recyclability of organic solvent with low surface tension. The drying kinetics were evaluated by analyzing the drying duration, moisture rates, and drying rates. Drying efficiency was assessed through density and dimensional stability after drying, to reflect the impacts on the porosity and microstructure of wood cells.

Materials and methods

Sample preparation

Japanese cedar (*Cryptomeria japonica*) was selected for this study because of its simple anatomical structure, which was suitable to be made lignin-free for subsequent drying parameter analysis.[13] Kyoto University provided small blocks of Japanese cedar, measuring $10 \times 10 \times 10\ mm^3$ in the radial, tangential, and longitudinal directions. Wood blocks of such dimensions were used to obtain homogeneous

delignification treatment results. Three specimens were oven-dried at 103 °C to determine the average initial moisture content and deduce the initial dry density of other wood specimens.[14]

Wood modification procedures

The wood delignification process combines organosolv treatment *via* alcoholysis and sodium chlorite bleaching. Portable reactors (TVS-N2 Type, Taiatsu Techno Corp, Japan) were used to perform alcoholysis in an oil bath, followed by sodium chlorite bleaching in beakers using a water bath (Figure 1).

For the alcoholysis of Japanese cedar wood, the stock solution consisted of ethylene glycol ($HOCH_2CH_2OH$) (Wako, Japan), distilled water, and 97% sulfuric acid (H_2SO_4) (Wako, Japan) was prepared in a mass ratio of 99:0.5:0.5. The wood blocks were first vacuum impregnated with the stock solution for 30 min before being heated at 150 °C for 1 h in a portable reactor. The reactor was placed in an oil bath, externally heated, and controlled *via* a combined stirring and a heating plate.[12] Excess reactants were removed from the samples by soaking in distilled water overnight following alcoholysis treatment. Organosolv by alcoholysis was coupled with sodium chlorite bleaching. Sodium chlorite bleaching, also known as the Wise method, has been conventionally used in the pulping industry.[15] The sodium chlorite solution was prepared by dissolving 1 g of sodium chlorite ($NaClO_2$) (Nacalai Tesque, Japan) in 150 mL of distilled water with the addition of 0.2 mL of acetic acid (Wako, Japan). The treated wood blocks from the previous step were treated in this solution in a 70 °C water bath for 8 h. Every hour, 1 g of $NaClO_2$ and 0.2 mL of acetic acid were added to the solution.

Drying techniques

Upon completion of the wood modification processes, the remaining chemical reagents and lignin fragments were removed from the samples by soaking in distilled water, fresh distilled water was replaced every few hours until the samples became colorless (Figure 1). The samples were subsequently subjected to different drying techniques.

To freeze-dry the modified samples as the control group, the delignified Japanese cedar was frozen using liquid nitrogen for 5 min, then freeze-dried at −45 °C and 15 Pa in an Eyela FDU-1200 freeze dryer. To study the effects of solvents and drying temperatures, the delignified Japanese cedar was soaked in either ethanol or acetone for 24–48 h to ensure thorough solvent impregnation into the pores. Fresh solvent was replaced frequently during the day (every 2 h) and left overnight, with the same replacement frequency the following day. The solvent-to-sample volume ratio was ∼10:1, providing sufficient dilution of residual water at each solvent change (Figure 1). Water-saturated samples without solvent exchange were used as controls. For ambient air drying, the samples were left in an ambient environment at room temperature. A laboratory oven was used to dry the samples at specified temperatures. Solvent boiling point drying was conducted at a heating temperature slightly above the boiling point of each solvent (i.e. 105 °C for water, 80 °C for ethanol, and 60 °C for acetone). Vacuum drying was performed by placing

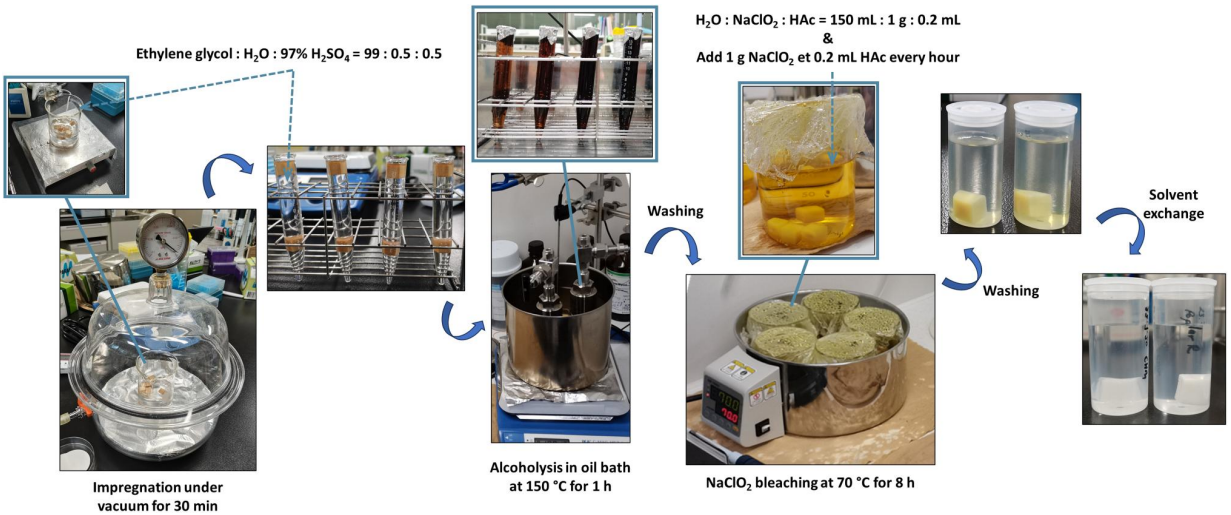

Figure 1. Delignification process of Japanese cedar wood blocks.

the samples in a desiccator connected to a vacuum pump at room temperature. To determine the optimal drying temperature for ethanol-exchanged colorless samples, two specimens were tested at each temperature: 26, 40, 60, 80, and 105 °C.

Characterization methods

Thin slices from both native and colorless wood samples were analyzed with Fourier transform infrared spectroscopy (FTIR) using a PerkinElmer Frontier system (Waltham, MA, USA) with an attenuated total reflection (ATR) accessory. Three FTIR spectra per specimen were acquired within the 4000–500 cm^{-1} range at 4 cm^{-1} resolution and averaged. The spectral pretreatments were performed by the ATR correction functions and normalized to the top absorbance band of the fingerprint region at ~1000 cm^{-1}.

The lignin content was estimated *via* a two-step acid hydrolysis method to determine the mass ratio of acid-insoluble substances. The wood specimens were ground and dissolved in 72% sulfuric acid (H_2SO_4) (Wako, Japan) at 30 °C for 1 h, then diluted to 4% and hydrolyzed in an autoclave at 121 °C for 1 h. After cooling, the precipitate and hydrolyzed solutions were separated by filtration using a glass funnel connected to a water aspirator. The acid-insoluble solid residue (Klason lignin) was dried at 105 °C in a weighing jar and quantified using Equation (1):

$$\text{Lignin content} = \frac{m_l}{m_s} \times 100\% \quad (1)$$

where m_l (mg) is the mass of the acid-insoluble precipitate (lignin) and m_s (mg) is the dry mass of the ground wood specimen placed into the acid solution.

The filtrate was neutralized with calcium carbonate and centrifuged before sugar analysis of the supernatant using a high-performance liquid chromatography (HPLC) system equipped with a separation column (Asahipak NH2P-50 4E, Showa Denko K.K., Tokyo, Japan), a differential refractive index detector, and an autosampler (Prominence, Shimadzu, Kyoto, Japan). The polysaccharide contents were calculated from each monosaccharide concentration using anhydrous correction factors, 0.90 for glucose, mannose, and galactose, 0.88 for xylose and arabinose.[13,16] The cellulose content was estimated by subtracting one-third of the mannan content from the glucan content, whereas the hemicellulose content was determined to be that of other non-cellulosic polysaccharides.[13] Two specimens were tested for both native and colorless wood, and the relative compositions of polysaccharides and acid-insoluble lignin were calculated, averaged, and normalized to 100%. These relative values were then converted to absolute compositions by multiplying them by the dry mass ratio after treatment.

X-ray diffractograms were obtained in reflection mode using an automated multipurpose X-ray diffractometer (SmartLab, Rigaku, Tokyo, Japan) operating at 40 kV and 30 mA. After performing background subtraction, the peak separations for cellulose I_β at (1–10), (110), and (200), corresponding to 2θ values of 14.6, 16.4, and 22.5°, respectively, along with the amorphous component at 18.5° were carried out using pseudo-Voigt function fitting to determine the crystalline index and the full width at half maximum (FWHM) for the (200) peak.[17,18]

The initial weight before treatment, humid weight after treatment, and final dry mass of the modified wood specimens were recorded with an analytical weighing balance (ViBRA HT) with a minimum reading of 0.0001 g. At the end of the experiments, all the wood specimens were dried in an oven at 103 °C until a stable mass was obtained.[14] The moisture content (M) was calculated using Equation (2):

$$M = \frac{m_t - m_d}{m_d} \quad (2)$$

where m_t (g) is the total mass of the specimen at time t, m_d (g) is the stabilized mass after oven drying at the end of the experiments.[19] Owing to the differences in the initial moisture content, the dimensionless moisture ratio (MR) was calculated using Equation (3) for a better comparison among samples:

$$MR = \frac{M_t - M_e}{M_0 - M_e} \quad (3)$$

where M_t, M_e, and M_0 are the moisture content at time t, the equilibrium moisture content, and the moisture content before drying, respectively.[19] When the weight change was insignificant at the end of the drying phase, the moisture content at that time was considered the equilibrium moisture content (M_e). For the drying temperature of 103 °C, M_e is zero, and $MR = M_t/M_0$. When MR is 0, the equilibrium moisture content is reached. The drying curves were plotted as MR against time.[20] The drying rate (DR) was calculated using Equation (4):[21]

$$DR = \frac{MR_0 - MR_f}{t} \quad (4)$$

where MR_0 and MR_f are the moisture ratios before and after drying, respectively, and t is the time interval. The drying rate curves were plotted as drying rate against moisture ratio.[20]

To assess the dimensional variation, the swelling and shrinkage behaviors of delignified wood were assessed by measuring three dimensions (radial, tangential, and longitudinal) with a micrometer at a precision of ±0.001 mm. The average of three measurements was taken for each dimension. Since the specimens swelled differently despite undergoing the same treatment, the shrinkages were calculated using Equations (5)–(7) to compare among them, based on the wet swollen dimensions which were measured just before the drying procedure.

$$\text{Longitudinal shrinkage} = \left(\frac{L_{wet} - L_{dry,f}}{L_{wet}}\right) \times 100\% \quad (5)$$

$$\text{Tangential shrinkage} = \left(\frac{T_{wet} - T_{dry,f}}{T_{wet}}\right) \times 100\% \quad (6)$$

$$\text{Radial shrinkage} = \left(\frac{R_{wet} - R_{dry,f}}{R_{wet}}\right) \times 100\% \quad (7)$$

where L, T, and R represent the longitudinal, tangential, and radial dimensions, respectively. The subscript "*dry,f*" refers to the final dimension after drying, and "*wet*" refers to the dimension of the wet specimen before drying.

The bulk density of the wood samples (g cm^{-3}) was calculated as the ratio of mass (g) to apparent volume (cm^3). The pore volume fraction was calculated with the dry wood sample density, ρ_{sample} and the density of the dry cell wall, $\rho_{cell\ wall}$ which is ~1.5 g cm^{-3} using Equation (8):[22]

$$\text{Pore volume fraction} = \left(1 - \frac{\rho_{sample}}{\rho_{cell\ wall}}\right) \times 100\% \quad (8)$$

Nitrogen sorption porosimetry was used to examine the SSA and porosity of the samples. Nitrogen sorption isotherms of the materials were measured using a Tristar II 3020 (Micromeritics) instrument. The specimens were outgassed at 40 °C for 5 h under a primary dynamic vacuum before measurement. The SSA and pore size distributions were estimated from the isotherms according to the Brunauer–Emmett–Teller (BET) theory and the Barrett–Joyner–Halenda (BJH) method.[23,24] The International Union of Pure and Applied Chemistry (IUPAC) classifies pore sizes into micropores (<2 nm), mesopores (2–50 nm), and macropores (>50 nm).

Results and discussions

The findings were divided into two parts: the assessment of delignification and the analysis of drying techniques. First, the effectiveness of removing non-cellulosic substances for delignification treatment involving organosolv and sodium chlorite bleaching was verified. The colorless lignin-free Japanese cedar samples, either water-saturated or solvent-exchanged (acetone or ethanol), were subsequently subjected to various drying conditions. Further examination of the ethanol-exchanged, lignin-free samples identified the optimal drying temperature resulting in minimal deformation.

Effect of the combined alcoholysis and sodium chlorite bleaching treatment

To ensure the removal of non-cellulosic substances without altering the natural hierarchical structure, the delignified Japanese cedar samples were freeze-dried and subjected to the following characterizations in comparison with native Japanese cedar.

Intensity changes in FTIR spectra

The cores of the wood specimens were analyzed using FTIR to determine structural and compositional similarities or differences. The results presented in Figure 2 allow to detect changes in chemical component content. After the treatment, the colorless wood samples exhibited significant variations in the intensity of several bands, notably those associated with lignin (1600, 1508, 1465, and 1264 cm^{-1}) and hemicelluloses (1730, 1240, and 808 cm^{-1}).[25] The disappearance of these peaks indicates the effective removal of lignin and hemicelluloses. A linear relationship has been reported between the area of the 1508 cm^{-1} band and lignin content but is difficult to directly correlate with the total lignin content in the cell wall.[26–28] The results related to each band match with the reported observations of delignified wood obtained by various delignification techniques.[5,11,29–32] Chemical component quantification can provide more information on such variation.

Chemical component quantification

The native and colorless Japanese cedar samples were analyzed for chemical component quantification using acid hydrolysis and a HPLC system. Acid-insoluble (Klason) lignin is the remaining solid residue after being treated with sulfuric acid in a two-step hydrolysis procedure that solubilized the carbohydrate component into monosaccharides.[33,34] In the native Japanese cedar wood samples, the acid-insoluble

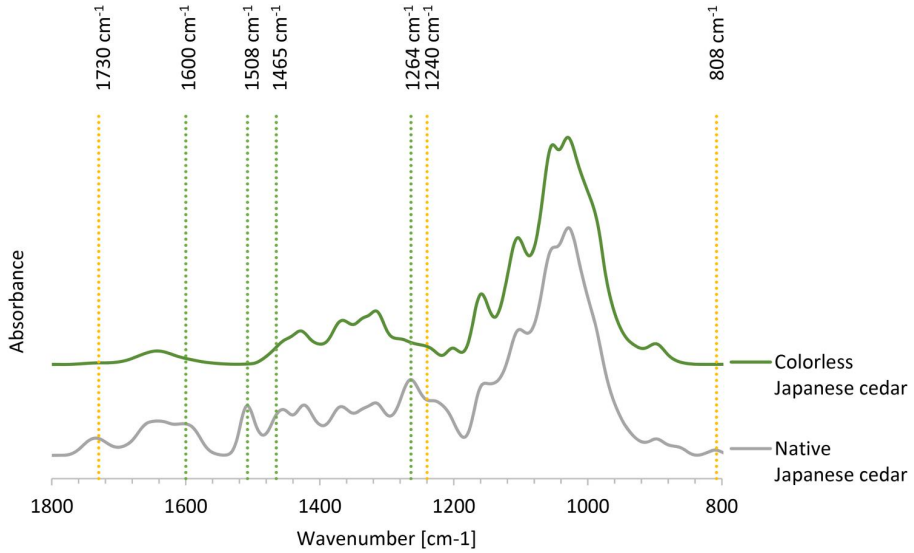

Figure 2. FTIR spectra for the cores of Japanese cedar wood blocks before and after delignification treatment.

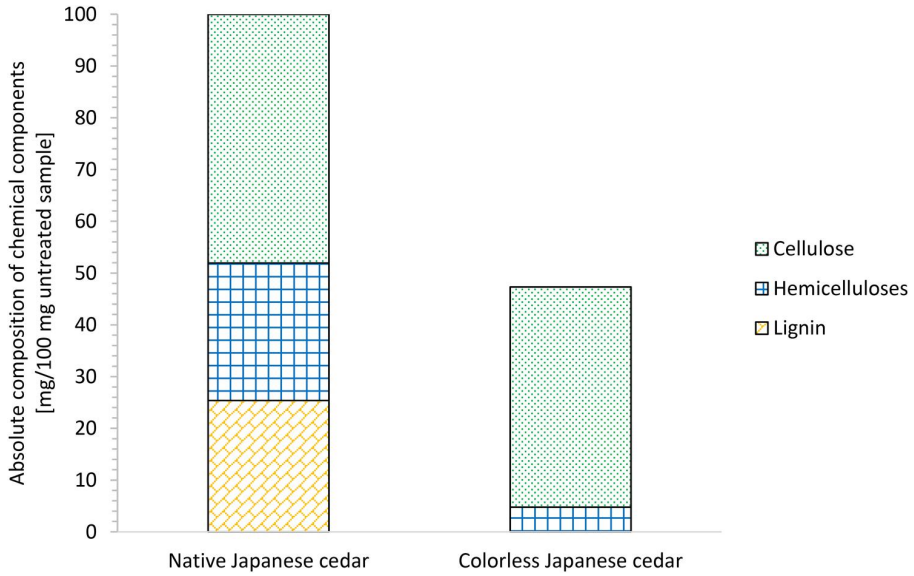

Figure 3. Ratio of chemical components in Japanese cedar wood before and after delignification treatment.

lignin comprised ~25% of its mass (Figure 3). The treated Japanese cedar showed significant removal of substances, especially acid-insoluble lignin. The consistently high glucose content suggests that cellulose remained largely unaffected by the treatment, with only lignin and hemicelluloses being preferentially altered. Similar findings were reported by Kurei et al. who conducted parametric studies of different delignification treatment conditions.[13]

X-ray diffraction analysis

The cellulose I polymorph remained unchanged in both native and colorless Japanese cedar samples, as observed in the wide-angle X-ray diffractograms. Similar patterns of distinct cellulose I_β peaks indicate that the natural cellulose crystalline structure was preserved (Figure 4). The higher crystalline index and lower FWHM for the (200) peak of colorless Japanese cedar, as calculated in Table 1, reflect the higher relative crystallinity due to the improved cellulose microfibril orientation post-treatment.[12] This increased crystallinity is correlated with the material strength and stability.

The alcoholysis procedure not only removed lignin by cleaving ether linkages but also hydrolyzed hemicelluloses. Subsequent sodium chlorite bleaching decomposed

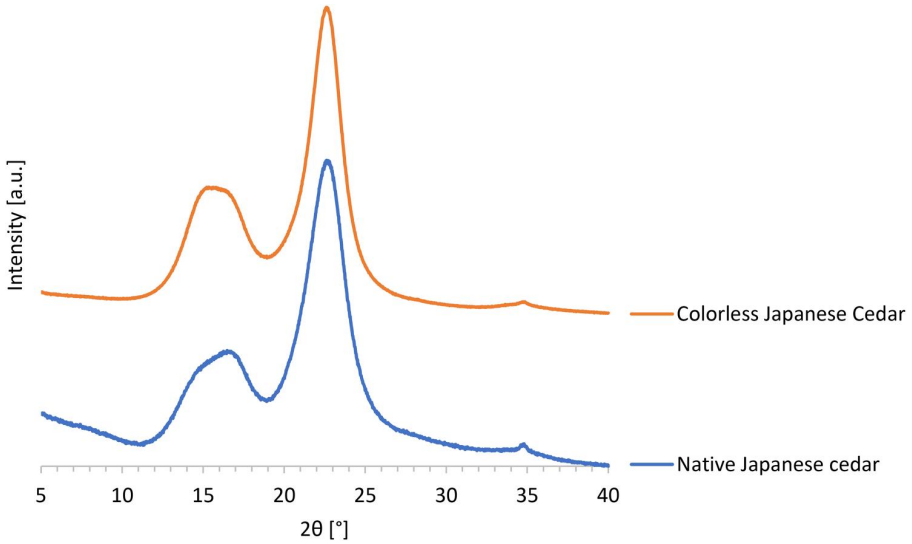

Figure 4. Normalized X-ray diffractograms of Japanese cedar wood blocks before and after delignification treatment.

Table 1. Crystalline index and full width at half maximum of native and colorless Japanese cedar samples.

Wood sample	Crystalline index	Full width at half maximum of (200) (°)
Native Japanese cedar	0.842	2.68
Colorless Japanese cedar	0.839	2.23

aromatic rings in lignin, providing wood with a colorless appearance.[17] This 2-step delignification treatment achieved the complete removal of lignin and chromophores while preserving the hierarchical structure and anatomical features of the wood.

Effect of solvent and drying conditions

After the final washing step, the modified wood became saturated with water. Direct oven drying of this water-saturated sample can cause significant shrinkage in the transverse (radial and tangential) direction due to the increase in capillary pressure during liquid evaporation. This pressure causes the cell wall to collapse and lose the created porosity, thereby increasing the density of the wood.[35] While freeze-drying is commonly used to remove water without altering the microstructure, it is impractical for industrial applications because of its high cost and high energy consumption.[36] Solvent exchange is a promising alternative, where the water within the wood cells is replaced with a liquid of lower surface tension, thus reducing the capillary pressure in the pores while drying. Repeated solvent exchanges using ethanol, isopropyl alcohol, hexane or *tert*-butanol have been reported to reduce the collapse and shrinkage of the porous structure during drying.[5,7,10,35] This study examines the impact of solvent type and heating temperature on the microstructure of cellulosic scaffolds.

After exchanging the water within the 1 cm^3 delignified Japanese cedar samples with ethanol or acetone, along with the non-exchanged samples, the samples were dried under three conditions: ambient, vacuum, and heated above the boiling point. The images of the resulting samples are presented in Table 2. The choice of solvent and drying conditions significantly affected the structure of delignified wood. Direct drying of the water-saturated samples resulted in obvious irregular shapes even not completely dried yet, regardless of the drying conditions. Exchanging water with ethanol or acetone better preserved the cubic shape of colorless Japanese cedar samples. The least deformation was observed for the ethanol-exchanged samples dried in an oven and under vacuum. In addition, ethanol is renewable and relatively eco-friendly compared with acetone, making it a promising solvent for this drying approach.

Drying kinetics

The evolution of the solvent moisture ratio under various drying conditions when different solvents were used is presented in Figures 5(a–c). To further explore how quickly the sample lost moisture with respect to the moisture ratio, the drying rates are illustrated in Figures 5(d–f). Generally, the drying rate decreased at lower moisture ratios. To compare the drying strategies with the ambient drying of water-saturated colorless wood, a constant measurement

Table 2. Images of delignified Japanese cedar samples dried under different conditions.

Type of solvent	Ambient drying	Boiling point oven drying	Vacuum drying
Water	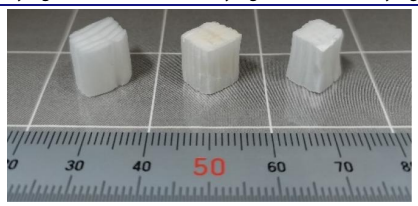		
Ethanol	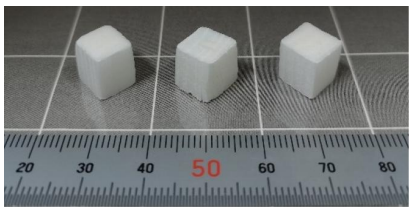		
Acetone	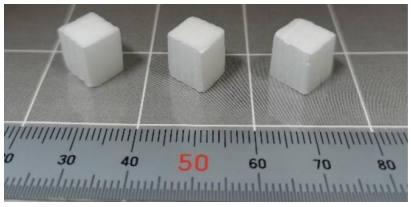		

frequency of 30 min was chosen. The highest drying rate occurred at the beginning of the drying process as the liquid on the outer surface evaporates first to the surrounding environment, whereas the inner moisture needs time to diffuse outwards for evaporation. The drying curves indicate that the most significant drop in moisture ratio occurs between the first two measurements, suggesting that shorter measurement intervals at the beginning would be useful for further comprehension of drying mechanisms of solvent-exchanged samples. For intermediate moisture ratios where data was unavailable, a smooth transition from high to low drying rates as the moisture ratio decreases is expected, as the reduced moisture content leaves less water available for evaporation, thus progressively slowing the drying process. Continuous measurements need to be implemented for future drying behavior prediction models.

The results indicated that direct ambient drying is the least efficient method, with water being the slowest to evaporate. Solvent exchange with ethanol or acetone greatly improves drying efficiency. The drying kinetics of ethanol and acetone were similar, as observed in Figures 5(b,c,e,f). Under ambient conditions, acetone evaporated faster due to its lower boiling point. Compared with atmospheric pressure, vacuum conditions further facilitated solvent evaporation compared to atmospheric pressure, significantly accelerating the drying process due to the reduced atmospheric pressure, which lowered the boiling point. The drying curves of solvent-exchanged samples steeply decreased to low moisture ratios by the first 30 min, similar to oven drying at temperature above the boiling point. Nevertheless, drying kinetics alone cannot guarantee the final quality of modified wood, and the dimensional variation must also be monitored.

Dimensional variation

The shrinkages and final dry density were compared to study the effects of different solvents and drying conditions. The oven temperatures were set slightly higher than each solvent's boiling temperature: 105 °C for water, 80 °C for ethanol, and 60 °C for acetone. As shown in Figure 6(a), the longitudinal length, corresponding to the axis of cellulose fiber, remained relatively stable across all the samples and drying methods, indicating that the drying process had a minimal impact. Sectional shrinkage, represented by the radial and tangential shrinkages shown in Figures 6(b,c), denotes cell wall collapse caused by capillary tension.

The lowest density was observed for H_2O freeze-dried samples, which was expected to best preserve the wood structure. Being the most commonly used drying technique reported in the literature, the freeze-dried colorless samples resulted in an increase in the pore volume fraction to 91% from 80% in native Japanese cedar wood. The density appeared to be lower for the freeze-drying method than for the other methods across all solvents, indicating better preservation of the porous structure. Following the freeze-dried water-saturated samples, the ethanol-exchanged sample dried at 80 °C had the second lowest density and least shrinkage in all directions, with a pore volume fraction of 89%. Ethanol and acetone appeared to result in low densities across all drying conditions, with vacuum and ambient conditions showed slightly higher densities. The ambient drying of the water-saturated delignified samples was incomplete, the accounted density had a high moisture content, and a much longer experiment time was needed to reach the equilibrium mass of the environment. However, high shrinkage in the radial direction was already observed even without reaching the equilibrium moisture content. The water-saturated delignified Japanese cedar samples dried in the oven and under vacuum had the highest densities and the greatest shrinkage in the

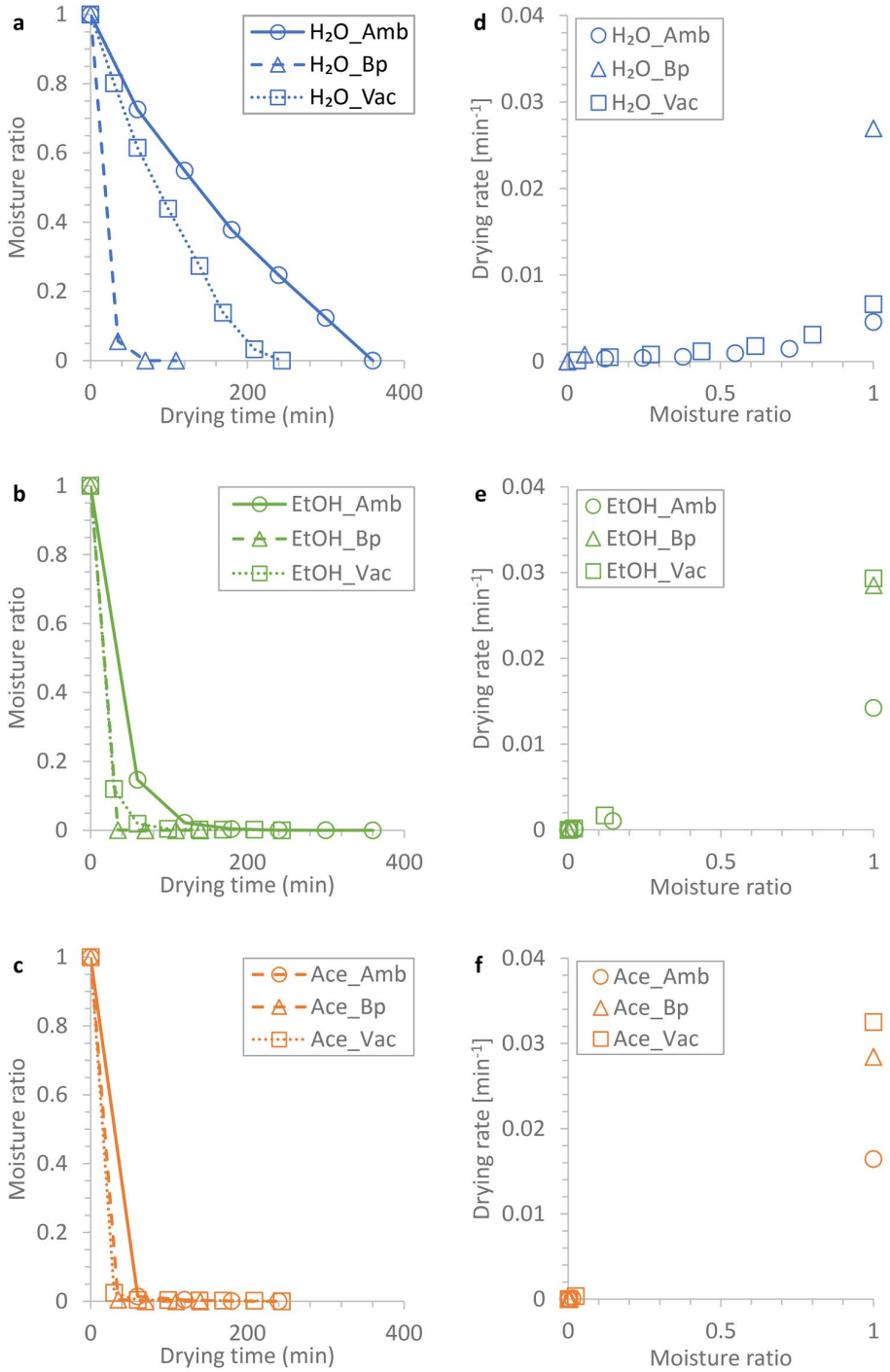

Figure 5. Drying curves (moisture ratio *vs.* drying time) for different solvents: water (a), ethanol (b), and acetone (c), and their respective drying rate curves (drying rate *vs.* moisture ratio) (d–f), under various drying conditions: ambient air drying (circles), boiling point drying (triangles), and vacuum drying (squares).

tangential and radial directions. These observations align with the reported literature.[37]

This study used the swollen volume after delignification as the initial reference volume (Figure 7), whereas literature data in Table 3 measured volumetric variations using the volume before delignification. This difference explains the volumetric expansion reported in freeze-dried delignified basswood.[37] Nevertheless, both findings indicated that freeze-drying effectively minimizes structural collapse. Samples dried from a water-saturated state, whether through oven-drying or vacuum drying, showed the highest

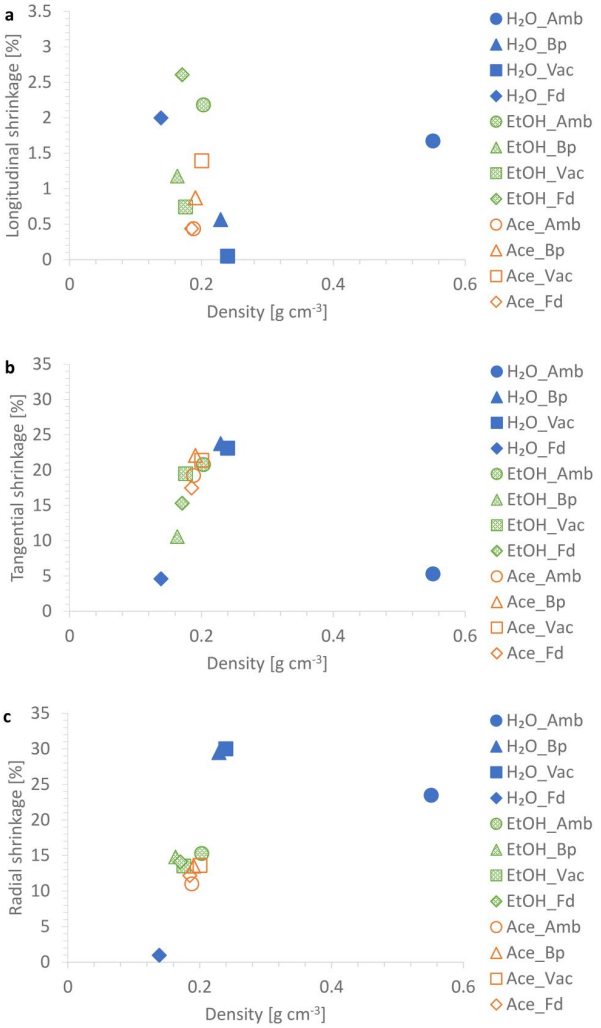

Figure 6. Dimensional shrinkage *vs.* density of delignified Japanese cedar samples dried with different solvents and drying environments in longitudinal (a), tangential (b), and radial (c) directions.

densities and greatest volumetric shrinkage, reflecting the high capillary tension generated during water evaporation. This pattern aligns with previous report of 50% shrinkage for water-saturated spruce dried under cyclic conditions at 65 °C.[38] In addition to freeze-drying, solvent-exchanged samples demonstrated less shrinkage compared to samples dried without solvent exchange, indicating that solvents like ethanol and acetone preserve porosity better than water, even without freeze-drying. Ethanol-dried colorless wood samples showed low volumetric shrinkage, suggesting that ethanol minimized capillary forces and structural collapse risk due to its lower surface tension. The choice of solvent and drying conditions significantly influenced the internal structure of wood, BET SSA analysis was performed on selected specimens to further assess their drying performance.

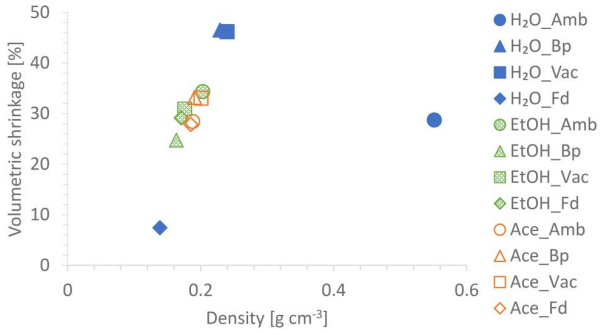

Figure 7. Volumetric shrinkage *vs.* density of delignified Japanese cedar dried with different solvents and drying environments.

Nitrogen adsorption

The nitrogen adsorption isotherm plotted in Figure 8 displays the quantity of nitrogen adsorbed (in $cm^3\ g^{-1}$ STP) as a function of relative pressure (P/P_0) for Japanese cedar samples dried under various conditions, providing insights into the porosity and surface area characteristics. The lowest adsorption was observed with untreated Japanese cedar samples across all relative pressures, indicating their limited porosity and SSA. After delignification, higher adsorption suggested the development of additional porosity. Ethanol exchange followed by drying at 80 °C resulted in the highest adsorption among all the samples, suggesting better preservation of new porosity. High adsorption was also observed with acetone as the solvent and drying at 60 °C. These results even surpassed those of the freeze-dried colorless samples. Despite the same delignification treatment that contributed to the creation of porosity, drying techniques significantly influenced the pore structure of wood. In general, the nitrogen adsorption-desorption capabilities of wood increase after delignification due to the high SSA of new nanoscale pores in cell wall for all the drying techniques tested. Better pore structure preservation could be achieved at the optimum drying temperature of a low surface tension solvent.

Brunauer–Emmett–Teller (BET) model was used to determine the SSA of the wood. Native Japanese cedar had a BET SSA of $3.1\ m^2\ g^{-1}$, which increased to $4.9\ m^2\ g^{-1}$ after delignification and classic freeze-drying. According to Figure 9, the BET SSA of samples varied considerably with solvent and drying conditions, affecting the microstructure of wood, which aligns with the findings of Fu et al.[9] Compared with native untreated wood, delignified wood subjected to all drying methods resulted in increased SSA, confirming again the contribution of delignification treatments to porosity development.

Table 3. Volumetric variation of different drying techniques involving delignified bulk wood.

Drying method	Delignifying method	Wood species	Volumetric variation of treated wood (%)	Ref.
Freeze-drying	$NaClO_2$ bleaching → Soda pulping	Basswood	+15.6	[37]
Air drying	$NaClO_2$ bleaching → Soda pulping	Basswood	−61.6	[37]
Solvent exchange to acetone 3 times, followed by hexane 3 times	$NaClO_2$ bleaching → Soda pulping	Basswood	−19.8	[37]
Cycled over 4 climate conditions before final drying at 65 °C	H_2O_2/Acetic acid bleaching	Spruce	−50	[38]

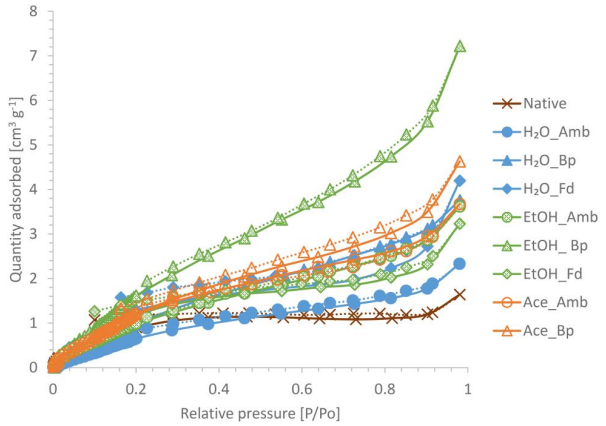

Figure 8. Adsorption-desorption isotherms of nitrogen of various wood specimens (solid line: adsorption; dotted line: desorption).

The ethanol-exchanged samples dried at 80 °C presented the highest SSA of 7.2 m^2 g^{-1}, demonstrating high porosity and suggesting that they have the best preservation of micropores and mesopores created during delignification. Compared with that at room temperature, the higher rate of moisture removal at 80 °C may have reduced the risk of collapse of the porous structure. Despite the excessive macroscale shrinkage of the water-saturated delignified samples dried at room temperature and 105 °C, the SSA remained higher than that of the native untreated wood, indicating the possible preservation of some newly created micro and mesopores in the collapsed cell wall lumen. In the case of room temperature drying, acetone yielded a higher SSA compared to ethanol and water. Both acetone and ethanol appeared to enhance the SSA of delignified wood more effectively, particularly when it was dried at boiling points. This could be due to their physical properties, such as lower surface tension and faster evaporation rates. Increased SSA benefits thermal conductivity reduction and provides a porous cellulosic scaffold for the impregnation of nanosized elements.

Compared with the literature summarized in Table 4, the reported SSA of treated wood varies depending on species, delignification methods, and drying techniques. For example, balsa wood, one of the most studied species, has a lower density than Japanese cedar, with high initial porosity that enhances the diffusion of delignifying solution, thus resuting in a higher SSA than the maximum observed in this study. A combination of delicate drying techniques, involving 96% ethanol and pure ethanol dehydration followed by supercritical CO_2 drying and freeze-drying, produced the highest SSA reported in the literature, reaching up to 41 m^2 g^{-1}. Our results indicated that, while some pore collapse occurred in colorless samples dried at atmospheric pressure, significant SSA was retained. Despite the more hydrophilic nature of the delignified cell wall, the use of solvents with low surface tension and rapid evaporation preserved the micro- and mesopores of colorless wood. This study's innovative approach, relying on optimizing solvent exchange and controlled drying conditions without freeze-drying, shows potential for scalable cellulosic scaffold preparation by reducing energy and equipment requirements while retaining porosity. The experimental results align with literature findings on the effect of delignification on porosity, while also highlighting the novel contribution of solvent-exchange strategies in enhancing SSA, presenting a promising alternative to freeze-drying.

The Barrett – Joyner – Halenda (BJH) calculation model was used to compare the influence of drying solvents and drying conditions on the pore size distribution. Most created pores after delignification fell below 2.5 nm, close to the micropore category (Figure 10), which is consistent with reported data.[41] In this pore diameter range, the highest pore volume was again observed in ethanol-exchanged samples dried at 80 °C, supporting the presence of abundant nanopores. Overall, the results implied that the choice of solvent and drying conditions can tune the microstructure of delignified wood, which is critical for optimizing wood properties for intended applications and industrial manufacturing decisions. In the subsequent experiments, ethanol was chosen as the exchange solvent.

Focus on different drying temperatures of ethanol-exchanged samples

Solvent exchange with ethanol before oven drying has been previously identified as a potential alternative to

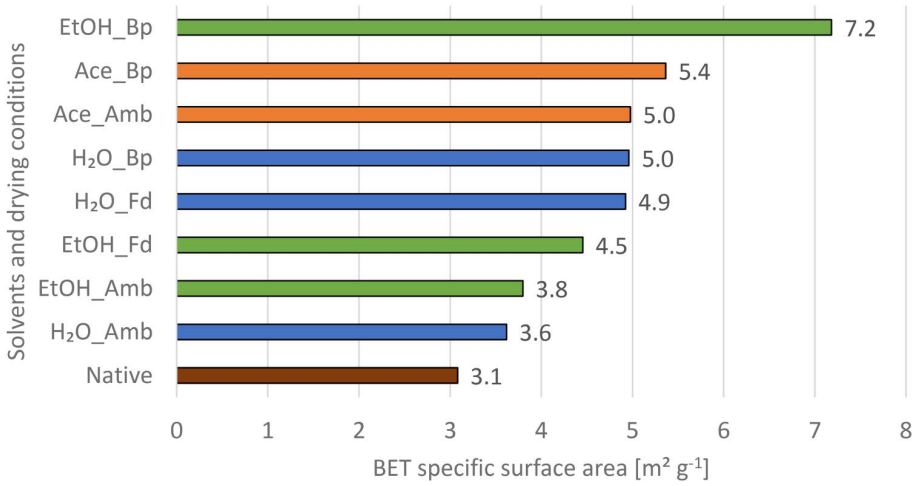

Figure 9. BET SSA of delignified Japanese cedar samples dried under different conditions in descending order.

Table 4. Different drying techniques involving delignified bulk wood.

Drying method	Delignifying method	Wood species	SSA of treated wood (m^2 g^{-1})	Ref.
Freeze-drying	Alkaline sulfite pulping → H_2O_2 bleaching	Balsa	13.8	[2]
	Freeze-drying	Peracetic acid bleaching	Balsa	9	[9]
	Freeze-drying	$NaClO_2$ bleaching	Balsa	40.5	[4]
Solvent exchange to ethanol, then 99.5% hexane	$NaClO_2$ bleaching	Balsa	37	[7]
Dehydration firstly with pure ethanol, then 1:1 mixture of ethanol and acetone, finally pure acetone, repeat 3 times	$NaClO_2$ bleaching	Balsa	19.8	[39]
Ethanol washing, followed by freeze-drying	$NaClO_2$ bleaching	Basswood	22.3	[40]
Solvent exchange with ethanol, acetone, and tert-butanol, followed by freeze-drying	Peracetic acid bleaching	Balsa	21	[9]
Dehydration by 96% ethanol and pure ethanol overnight, then dried by supercritical drying in CO_2, followed by freeze-drying	Peracetic acid bleaching	Balsa	41	[9]

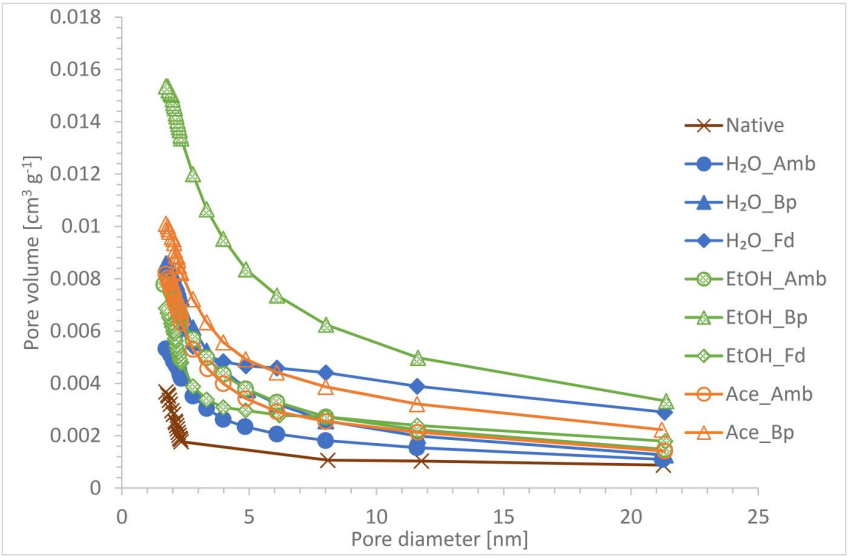

Figure 10. Pore volume distributions of various wood specimens.

freeze-drying. However, the dimensions of samples dried without freeze-drying were not as well-preserved as those in freeze-dried samples, resulting in slightly higher densities. When liquid within the pores begins to evaporate, capillary pressure is generated, as described by the Laplace law (Equation 9).

$$P_{cap} = \frac{2\gamma\cos\theta}{a} \tag{9}$$

where P_{cap} is the capillary pressure in the pore, γ the liquid's surface tension, θ the contact angle, and a the pore radius. After delignification, not only there were more small-sized pores, the contact angle was also reported to be lower, contributing to higher capillary pressures that elevate the risk of collapse.[42] While using solvents with lower surface tension can reduce capillary pressure, drying at elevated temperatures during the early drying stages might lead to moisture gradients across the material, resulting in drying stress and internal crushing in the partially liquid-filled cells. Therefore, identifying the optimal drying temperature is crucial. This section seeks to demonstrate the influence of temperature through determination of optimal drying temperature for ethanol-exchanged colorless Japanese cedar samples which better maintains dimensional stability. Following delignification, samples were solvent-exchanged with ethanol and dried at various temperatures.

The results in Figures 11 and 12 showed that increasing the heating temperature reduces the moisture ratio more rapidly, thereby contributing to a higher drying rate. The drying rate curves adhered to the common trend in drying processes, where the rate of moisture loss was high at the beginning and decreased as the wood dries. Drying at room temperature (26 °C) and lower oven temperature (40 °C) resulted in a gradual decrease in moisture content over time. Drying at 60 and 105 °C was the fastest, but the primary focus was on the dimensional stability and BET SSA instead of the drying speed.

Noting that the boiling point of ethanol is 78 °C, drying at 80 °C was particularly interesting. This temperature resulted in a slower drying process than 60 and 105 °C, but it maintained a longer period of efficient solvent evaporation before the drying rate decreased. A lower drying rate implied less stress on the wood structure, which correlated with reduced dimensional changes in samples dried at 80 °C, as shown in Figure 13. The ideal drying temperature for ethanol-exchanged delignified Japanese cedar must balance drying kinetics with the preservation of wood dimensions and porosity.

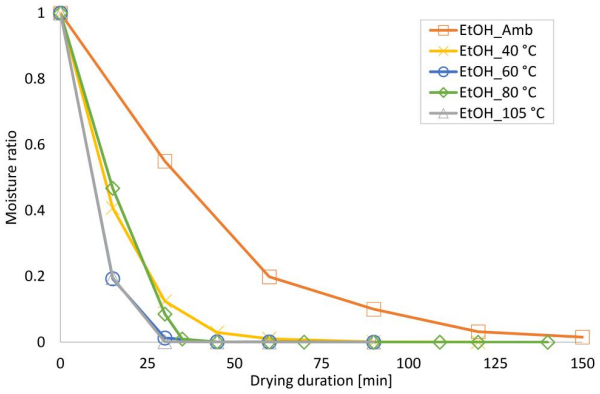

Figure 11. Drying curves (moisture ratio *vs.* drying duration) of ethanol-exchanged delignified Japanese cedar samples.

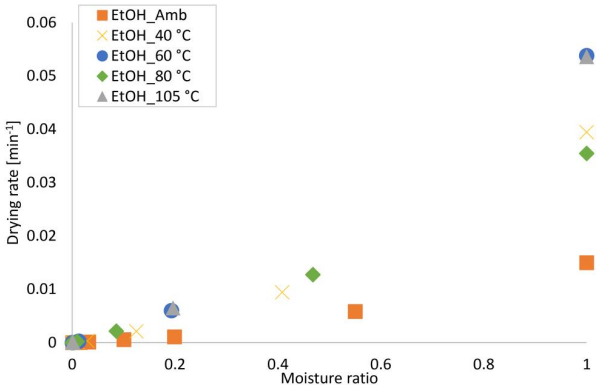

Figure 12. Drying rate curves (drying rate *vs.* moisture ratio) of ethanol-exchanged delignified Japanese cedar samples.

The dimensional stability and density of delignified Japanese cedar wood after ethanol exchange and subsequent drying at different temperatures are presented in Figure 13. The longitudinal shrinkages were below 2%, indicating that the cellulose fiber length was not much affected by drying. The tangential and radial dimensions showed varying degrees of shrinkage. Notably, the least tangential and radial shrinkages occurred at 80 °C, resulting in the lowest density among the other temperatures. This again suggests that heating close to the boiling point of ethanol is optimal for drying ethanol-exchanged colorless Japanese cedar samples, as it resulted in minimal sectional shrinkage. The drying temperature of 80 °C appeared to be a balance between high drying efficiency without excessive shrinkage, making it particularly advantageous for industrial applications aimed at producing low-density modified wood. These observations also suggested that the drying process of delignified wood needs to be carefully manipulated in terms of both the solvent evaporation efficiency and the final product quality.

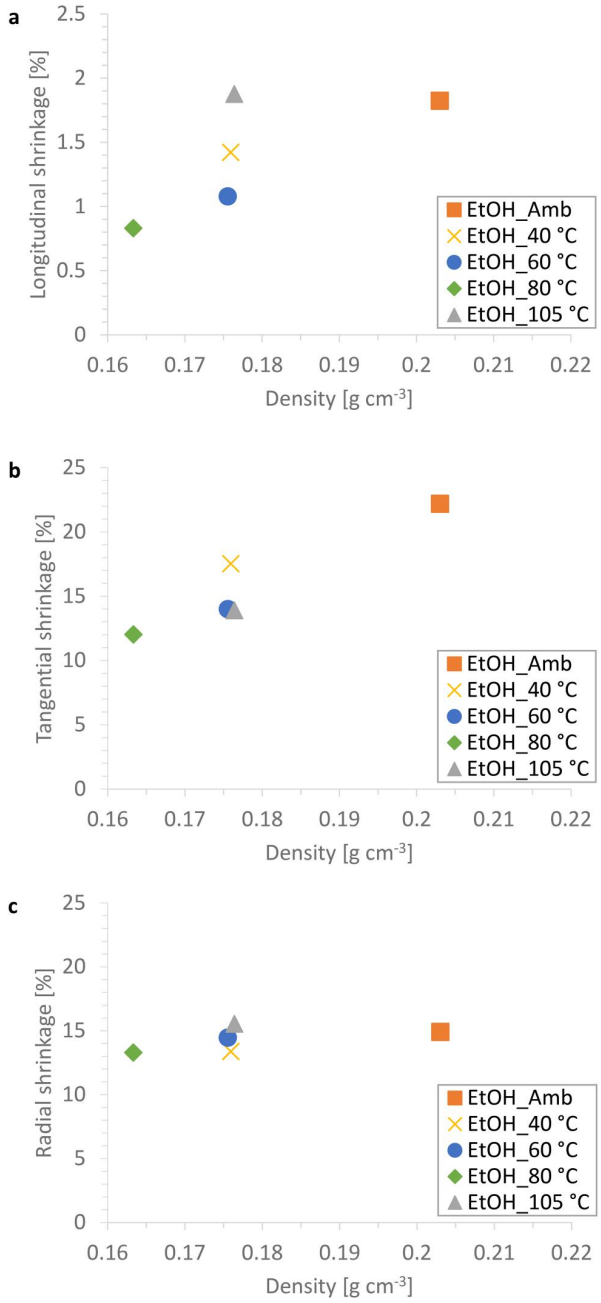

Figure 13. Dimensional shrinkage *vs.* density of delignified ethanol-exchanged Japanese cedar samples dried under different environments in longitudinal (a), tangential (b), and radial (c) directions.

Strengths and limitations

Wood modification by the removal of non-cellulosic substances has been shown to change its composition without affecting the properties of cellulose microfibrils. The organosolv process by alcoholysis, followed by sodium chlorite bleaching, efficiently removed lignin and resulted in a highly porous structure with a low density for improved insulation properties. Delignification treatment creates two types of porosity: "nanoporosity" within the cell wall that is detectable *via* BET SSA measurements, and "microcracks" created by the enlargement of small pores along with the separation of middle lamella with high lignin content at the corners of the cell wall, observed by scanning electron microscopy.[9] The removal of lignin can be compared to the absence of concrete in reinforced bars, leaving cellulose microfibrils without a binding agent, which deteriorates the mechanical properties and increases the risk of defibrillation.

Based on the experimental results, each drying technique has its advantages and disadvantages. As the modified wood is more susceptible to dimensional changes during the subsequent drying, the drying environment for solvent evaporation is crucial for maintaining the microstructure of cellulose microfibrils. Proper drying ensures that these pores are filled with air with low thermal conductivity, contributing to a lower effective thermal conductivity of the modified wood. By tailoring the drying process, the dimensional and physical properties of the wood microstructure after chemical modification can be retained as needed.

Further experiments are necessary to observe the cellulose behavior during drying. In addition, more data points at shorter time intervals are needed for a better understanding of drying kinetics. The drying technique should balance the drying time and preservation of the delignified wood structure. To maintain structural integrity with minimum shrinkage, ethanol solvent exchange followed by drying at 80 °C seems to be the most effective method. This is important when the low density of the functional wood scaffold is the key consideration. In contrast, higher temperatures can accelerate moisture removal. Indeed, shrinkage issues might be solved simply with large-scale freeze-drying or supercritical drying instruments.

Conclusion and perspectives

In this study, various drying techniques for colorless Japanese cedar wood were investigated for the first time, aiming to optimize the preservation of its porous structure and improve scalability for industrial applications. The combined alcoholysis and sodium chlorite bleaching treatment effectively removed lignin and hemicelluloses while preserving the cellulosic structure, resulting in highly porous delignified wood. Solvent exchange with a low-surface-tension solvent (ethanol or acetone) before drying significantly

improved dimensional stability and porosity retention at ambient conditions compared to drying water-saturated samples. Among the drying methods tested, ethanol-exchanged samples dried at 80 °C (near ethanol's boiling point) showed the best balance of drying efficiency and microstructure preservation, achieving minimal shrinkage and a high specific surface area (7.2 m^2 g^{-1}). This solvent exchange and controlled temperature drying approach represents a promising, energy-efficient alternative to freeze-drying for industrial-scale production of cellulose scaffolds, which have potential applications in developing bio-based thermal insulators and other functional materials. By interpreting the relationships between drying conditions, dimensional stability, and porosity, this study provides valuable guidance for industrial implementation of delignified wood production, balancing efficiency and quality while reducing energy consumption. Future work should further assess the mechanical and thermal properties of the delignified wood to fully evaluate their suitability for advanced applications. Additional research on optimizing drying processes through experimental and numerical studies at various temperatures and airflow rates, as well as exploring combined drying methods, such as electromagnetic waves, forced convection, or infrared, could open new pathways for innovative use of colorless wood in materials science and engineering.

Nomenclature

a	pore radius (m)
Amb	ambient drying
Bp	boiling point drying
DR	drying rate (min^{-1})
Fd	freeze-drying
L	longitudinal direction
M	moisture content of wood specimen (–)
M_0	moisture content before drying (–)
m_d	final stabilized mass after oven drying at 105 °C (g)
M_e	equilibrium moisture content (–)
m_l	mass of acid-insoluble precipitate (lignin) (g)
MR	moisture ratio (–)
MR_0	moisture ratio before drying (–)
MR_f	moisture ratio after drying (–)
m_s	dry mass of the ground wood specimen placed into the acid solution (g)
m_t	total mass of the specimen at time t (g)
M_t	moisture content at time t (–)
P_{cap}	capillary pressure (Pa)
R	radial direction
SSA	specific surface area (m^2 g^{-1})
T	tangential direction
Vac	vacuum drying
γ	surface tension (N m^{-1})
θ	contact angle (rad)
$\rho_{cell\ wall}$	density of dry cell wall (g cm^{-3})
ρ_{sample}	dry wood sample density (g cm^{-3})

Acknowledgments

The authors extend their gratitude to Y. Nishiyama for fruitful discussions that led to the consideration of solvent exchange as a drying strategy. The authors also wish to thank F. Gros, F. Brun, F. Audonnet, C. Gardarin, T. Kurei, X. Wei, Y. Yasuda, A. Yamanaka, S. Sakai, and R. Suzuki for their assistance with experimental instrumentation.

Disclosure statement

The authors report no conflicts of interest. The authors alone are responsible for the content and writing of the paper.

Funding

This work was supported by the French National Research Agency (ANR) and the company Dagard, under the "France Relance" plan. A research visit to Japan was co-funded by the I-Site project CAP 20-25 and the Tokyo University of Agriculture and Technology.

References

[1] Dagnachew, A. G.; Hof, A.; van Soest, H.; Vuuren, D. Climate change measures and sustainable development goals. *PBL Netherlands Environmental Assessment Agency: The Hague*, **2021**.

[2] Song, J.; Chen, C.; Yang, Z.; Kuang, Y.; Li, T.; Li, Y.; Huang, H.; Kierzewski, I.; Liu, B.; He, S.; et al. Highly Compressible, Anisotropic Aerogel with Aligned Cellulose Nanofibers. *ACS Nano* **2018**, *12*, 140–147. DOI: 10.1021/acsnano.7b04246.

[3] Li, T.; Song, J.; Zhao, X.; Yang, Z.; Pastel, G.; Xu, S.; Jia, C.; Dai, J.; Chen, C.; Gong, A.; et al. Anisotropic, Lightweight, Strong, and Super Thermally Insulating Nanowood with Naturally Aligned Nanocellulose. *Sci. Adv.* **2018**, *4*, eaar3724. DOI: 10.1126/sciadv.aar3724.

[4] Garemark, J.; Perea-Buceta, J. E.; Rico del Cerro, D.; Hall, S.; Berke, B.; Kilpeläinen, I.; Berglund, L. A.; Li, Y. Nanostructurally Controllable Strong Wood Aerogel toward Efficient Thermal Insulation. *ACS Appl. Mater. Interfaces* **2022**, *14*, 24697–24707. DOI: 10.1021/acsami.2c04584.

[5] Zhao, X.; Liu, Y.; Zhao, L.; Yazdkhasti, A.; Mao, Y.; Siciliano, A. P.; Dai, J.; Jing, S.; Xie, H.; Li, Z.; et al. A Scalable High-Porosity Wood for Sound Absorption and Thermal Insulation. *Nat. Sustain.* **2023**, *6*, **306**–315. DOI: 10.1038/s41893-022-01035-y

[6] Vitas, S.; Segmehl, J.; Burgert, I.; Cabane, E. Porosity and Pore Size Distribution of Native and Delignified Beech Wood Determined by Mercury Intrusion Porosimetry. *Materials* **2019**, *12*, 416. DOI: 10.3390/ma12030416.

[7] Wang, S.; Li, L.; Zha, L.; Koskela, S.; Berglund, L. A.; Zhou, Q. Wood Xerogel for Fabrication of High-Performance Transparent Wood. *Nat. Commun.* **2023**, *14*, 2827. DOI: 10.1038/s41467-023-38481-x.

[8] Fu, Q. *Wood Nanotechnologies for Transparency, Fire Retardancy and Liquid Separation*; Royal Institute of Technology: Stockholm, **2018**.

[9] Fu, Q.; Medina, L.; Li, Y.; Carosio, F.; Hajian, A.; Berglund, L. A. Nanostructured Wood Hybrids for Fire-Retardancy Prepared by Clay Impregnation into the Cell Wall. *ACS Appl. Mater. Interfaces* **2017**, *9*, 36154–36163. DOI: 10.1021/acsami.7b10008.

[10] Sakuma, W.; Yamasaki, S.; Fujisawa, S.; Kodama, T.; Shiomi, J.; Kanamori, K.; Saito, T. Mechanically Strong, Scalable, Mesoporous Xerogels of Nanocellulose Featuring Light Permeability, Thermal Insulation, and Flame Self-Extinction. *ACS Nano* **2021**, *15*, 1436–1444. DOI: 10.1021/acsnano.0c08769.

[11] He, S.; Chen, C.; Li, T.; Song, J.; Zhao, X.; Kuang, Y.; Liu, Y.; Pei, Y.; Hitz, E.; Kong, W.; et al. An Energy-Efficient, Wood-Derived Structural Material Enabled by Pore Structure Engineering towards Building Efficiency. *Small Methods* **2020**, *4*, 1900747.

[12] Horikawa, Y.; Tsushima, R.; Noguchi, K.; Nakaba, S.; Funada, R. Development of Colorless Wood via Two-Step Delignification Involving Alcoholysis and Bleaching with Maintaining Natural Hierarchical Structure. *J. Wood Sci.* **2020**, *66*, 37.

[13] Kurei, T.; Sakai, S.; Nakaba, S.; Funada, R.; Horikawa, Y. Structural and Mechanical Roles of Wood Polymer Assemblies in Softwood Revealed by Gradual Removal of Polysaccharides or Lignin. *Int. J. Biol. Macromol.* **2024**, *259*, 129270. DOI: 10.1016/j.ijbiomac.2024.129270.

[14] AFNOR. Moisture Content of a Piece of Sawn Timber. Part 1: Determination by Oven Dry Method, *NF EN 13183-1*. Paris: AFNOR, **2002**.

[15] Wise, L. E.; Murphy, M.; Adieco, A. A. D. *A Chlorite Holocellulose, Its Fractionation and Bearing on Summative Wood Analysis and on Studies on the Hemicelluloses*; *Paper Trade Journal,* New York, NY, **1946**; Vol. 122, pp 35.

[16] Liao, H.; You, J.; Wen, P.; Ying, W.; Yang, Q.; Xu, Y.; Zhang, J. Production of monosaccharides from poplar by a two-step hydrogen peroxide-acetic acid and sodium hydroxide pretreatment. *Ind. Crops Prod.* **2021**, *170*, 113820.

[17] Hirano, S.; Kurei, T.; Nakaba, S.; Funada, R.; Horikawa, Y. Elucidation of Alcoholysis for the Preparation of Lignin-Free Wood Sections from *Cryptomeria japonica*. *Cellulose* **2023**, *30*, 6589–6600. DOI: 10.1007/s10570-023-05291-9.

[18] Park, S.; Baker, J. O.; Himmel, M. E.; Parilla, P. A.; Johnson, D. K. Cellulose Crystallinity Index: Measurement Techniques and Their Impact on Interpreting Cellulase Performance. *Biotechnol. Biofuels* **2010**, *3*, 10. DOI: 10.1186/1754-6834-3-10.

[19] Naderinezhad, S.; Etesami, N.; Poormalek Najafabady, A.; Ghasemi Falavarjani, M. Mathematical Modeling of Drying of Potato Slices in a Forced Convective Dryer Based on Important Parameters. *Food Sci. Nutr.* **2016**, *4*, 110.

[20] Timofeev, O. N.; Jetsu, P.; Keränen, J. T. Drying of Thick Foam Formed Mats Comprising Chemithermomechanical Pulp Fibers. *BioResources* **2022**, *17*, 2547–2562. DOI: 10.15376/biores.17.2.2547-2562.

[21] Timofeev, O.; Jetsu, P.; Kiiskinen, H.; Keränen, J. T. Drying of Foam-Formed Mats from Virgin Pine Fibers. *Dry. Technol.* **2016**, *34*, 1210.

[22] Kollmann, F. F. P.; Côté, W. A. *Principles of Wood Science and Technology*; Springer-Verlag: Berlin, **1968**.

[23] Liang, R.; Zhu, Y.-H.; Wen, L.; Zhao, W.-W.; Kuai, B.-B.; Zhang, Y.-L.; Cai, L.-P. Exploration of Effect of Delignification on the Mesopore Structure in Poplar Cell Wall by Nitrogen Absorption Method. *Cellulose* **2020**, *27*, 1921–1932. DOI: 10.1007/s10570-019-02921-z.

[24] Quirk, J. P. Significance of Surface Areas Calculated from Water Vapor Sorption Isotherms by Use of the B.E.T. Equation. *Soil Sci.* **1955**, *80*, 423.

[25] Horikawa, Y.; Hirano, S.; Mihashi, A.; Kobayashi, Y.; Zhai, S.; Sugiyama, J. Prediction of Lignin Contents from Infrared Spectroscopy: Chemical Digestion and Lignin/Biomass Ratios of *Cryptomeria japonica*. *Appl. Biochem. Biotechnol.* **2019**, *188*, 1066–1076. DOI: 10.1007/s12010-019-02965-8.

[26] Rodrigues, J.; Faix, O.; Pereira, H. Determination of Lignin Content of Eucalyptus Globulus Wood Using FTIR Spectroscopy. *Holzforschung* **1998**, *52*, 46–50. DOI: 10.1515/hfsg.1998.52.1.46.

[27] Pandey, K. K. A Study of Chemical Structure of Soft and Hardwood and Wood Polymers by FTIR Spectroscopy. *J. Appl. Polym. Sci.* **1999**, *71*, 1969.

[28] Hatfield, R.; Fukushima, R. S. Can Lignin Be Accurately Measured? *Crop Sci.* **2005**, *45*, 832.

[29] Wu, Y.; Wu, J.; Yang, F.; Tang, C.; Huang, Q. Effect of H_2O_2 Bleaching Treatment on the Properties of Finished Transparent Wood. *Polymers* **2019**, *11*, 776. DOI: 10.3390/polym11050776.

[30] Shi, J.; Peng, J.; Huang, Q.; Cai, L.; Shi, S. Q. Fabrication of Densified Wood via Synergy of Chemical Pretreatment, Hot-Pressing and Post Mechanical Fixation. *J. Wood Sci.* **2020**, *66*, 5.

[31] Vay, O.; Busquets-Ferrer, M.; Emsenhuber, G.; Huber, C.; Gindl-Altmutter, W.; Hansmann, C. Thermal Conductivity of Untreated and Chemically Treated Poplar Bark and Wood. *Holzforschung* **2021**, *75*, 1125–1135. DOI: 10.1515/hf-2020-0268.

[32] Siciliano, A. P.; Zhao, X.; Fedderwitz, R.; Ramakrishnan, K.; Dai, J.; Gong, A.; Zhu, J. Y.; Kośny, J.; Hu, L. Sustainable Wood-Waste-Based Thermal Insulation Foam for Building Energy Efficiency. *Buildings* **2023**, *13*, 840. DOI: 10.3390/buildings13040840.

[33] Dence, C. W. The Determination of Lignin. In *Methods in Lignin Chemistry*; Lin, S. Y., Dence, C. W., Eds.; Springer: Berlin; Heidelberg, **1992**; pp 33–61.

[34] Yuan, T.; Zeng, J.; Wang, B.; Cheng, Z.; Chen, K. Lignin Containing Cellulose Nanofibers (LCNFs): Lignin Content-Morphology-Rheology Relationships.

Carbohydr. Polym. **2021**, *254*, 117441. DOI: 10.1016/j.carbpol.2020.117441.

[35] Wang, Q.; Yao, Q.; Liu, J.; Sun, J.; Zhu, Q.; Chen, H. Processing Nanocellulose to Bulk Materials: A Review. *Cellulose* **2019**, *26*, 7585–7617. DOI: 10.1007/s10570-019-02642-3.

[36] Panzarasa, G.; Burgert, I. Designing Functional Wood Materials for Novel Engineering Applications. *Holzforschung* **2022**, *76*, 211–222. DOI: 10.1515/hf-2021-0125.

[37] Han, X.; Ye, Y.; Lam, F.; Pu, J.; Jiang, F. Hydrogen-Bonding-Induced Assembly of Aligned Cellulose Nanofibers into Ultrastrong and Tough Bulk Materials. *J. Mater. Chem. A* **2019**, *7*, 27023–27031. DOI: 10.1039/C9TA11118B.

[38] Segmehl, J.; Studer, V.; Keplinger, T.; Burgert, I. Characterization of Wood Derived Hierarchical Cellulose Scaffolds for Multifunctional Applications. *Materials* **2018**, *11*, 517. DOI: 10.3390/ma11040517.

[39] Li, Y.; Fu, Q.; Yu, S.; Yan, M.; Berglund, L. Optically Transparent Wood from a Nanoporous Cellulosic Template: Combining Functional and Structural Performance. *Biomacromolecules* **2016**, *17*, 1358–1364. DOI: 10.1021/acs.biomac.6b00145.

[40] Jia, C.; Jiang, F.; Hu, P.; Kuang, Y.; He, S.; Li, T.; Chen, C.; Murphy, A.; Yang, C.; Yao, Y.; et al. Anisotropic, Mesoporous Microfluidic Frameworks with Scalable, Aligned Cellulose Nanofibers. *ACS Appl. Mater. Interfaces* **2018**, *10*, 7362–7370. DOI: 10.1021/acsami.7b17764.

[41] Fu, Q.; Ansari, F.; Zhou, Q.; Berglund, L. A. Wood Nanotechnology for Strong, Mesoporous, and Hydrophobic Biocomposites for Selective Separation of Oil/Water Mixtures. *ACS Nano* **2018**, *12*, 2222–2230. DOI: 10.1021/acsnano.8b00005.

[42] Chen, Z.; Dang, B.; Luo, X.; Li, W.; Li, J.; Yu, H.; Liu, S.; Li, S. Deep Eutectic Solvent-Assisted In Situ Wood Delignification: A Promising Strategy To Enhance the Efficiency of Wood-Based Solar Steam Generation Devices. *ACS Appl. Mater. Interfaces* **2019**, *11*, 26032–26037. DOI: 10.1021/acsami.9b08244.